

JWST/NIRSpec detection of complex structures in Saturn's sub-auroral ionosphere and stratosphere

Article

Published Version

Creative Commons: Attribution 4.0 (CC-BY)

Open Access

Stallard, T. S., Moore, L., Melin, H., Agiwal, O., Nahid Chowdhury, M., Johnson, R. E., Knowles, K. L., Thomas, E. M., Tiranti, P. I., O'Donoghue, J. ORCID: <https://orcid.org/0000-0002-4218-1191>, Mohamed, K., Mueller-Wodarg, I., Fletcher, L., de Pater, I., Fouchet, T. and Badman, S. V. (2025) JWST/NIRSpec detection of complex structures in Saturn's sub-auroral ionosphere and stratosphere. *Geophysical Research Letters*, 52 (17). e2025GL116491. ISSN 0094-8276 doi: 10.1029/2025GL116491 Available at <https://centaur.reading.ac.uk/124135/>

It is advisable to refer to the publisher's version if you intend to cite from the work. See [Guidance on citing](#).

To link to this article DOI: <http://dx.doi.org/10.1029/2025GL116491>

Publisher: American Geophysical Union

All outputs in CentAUR are protected by Intellectual Property Rights law, including copyright law. Copyright and IPR is retained by the creators or other copyright holders. Terms and conditions for use of this material are defined in

the [End User Agreement](#).

www.reading.ac.uk/centaur

CentAUR

Central Archive at the University of Reading

Reading's research outputs online

Geophysical Research Letters[®]



RESEARCH LETTER

10.1029/2025GL116491

Key Points:

- Saturn's sub-auroral ionosphere contains a string of dark beads surrounded by bright halos, equatorward of Enceladus's ionospheric footprint
- These dark beads are most likely the result of thermospheric dynamics driven by ionospheric winds
- The underlying non-LTE methane emission contains a unique morphology indicating complex dynamics in this region

Supporting Information:

Supporting Information may be found in the online version of this article.

Correspondence to:

T. S. Stallard,
tom.stallard@northumbria.ac.uk

Citation:

Stallard, T. S., Moore, L., Melin, H., Agiwal, O., Chowdhury, M. N., Johnson, R. E., et al. (2025). JWST/NIRSpec detection of complex structures in Saturn's sub-auroral ionosphere and stratosphere. *Geophysical Research Letters*, 52, e2025GL116491. <https://doi.org/10.1029/2025GL116491>

Received 22 APR 2025

Accepted 5 AUG 2025

Author Contributions:

Conceptualization: Tom S. Stallard,

Luke Moore, M. Nahid Chowdhury

Data curation: Tom S. Stallard,

Henrik Melin

Formal analysis: Tom S. Stallard,

Henrik Melin

Funding acquisition: Tom S. Stallard,

Luke Moore

Investigation: Tom S. Stallard,

Luke Moore, Henrik Melin,

James O'Donoghue, Imke de Pater

Methodology: Tom S. Stallard,

Henrik Melin, Leigh Fletcher

Project administration: Tom S. Stallard

Software: Tom S. Stallard, Henrik Melin



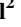
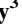
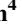





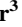



Validation: Tom S. Stallard

© 2025. The Author(s).

This is an open access article under the terms of the [Creative Commons Attribution License](https://creativecommons.org/licenses/by/4.0/), which permits use,

distribution and reproduction in any medium, provided the original work is properly cited.

JWST/NIRSpec Detection of Complex Structures in Saturn's Sub-Auroral Ionosphere and Stratosphere

Tom S. Stallard¹ , Luke Moore² , Henrik Melin¹, Omakshi Agiwal² , M. Nahid Chowdhury³ , Rosie E. Johnson⁴ , Katie L. Knowles¹ , Emma M. Thomas¹ , Paola I. Tiranti¹ , James O'Donoghue⁵ , Khalid Mohamed², Ingo Mueller-Wodarg⁶ , Leigh Fletcher³ , Imke de Pater⁷ , Thierry Fouchet⁸ , and Sarah V. Badman⁹ 

¹Department of Maths, Physics, and Electrical Engineering, Northumbria University, Newcastle Upon Tyne, UK, ²Center for Space Physics, Boston University, Boston, MA, USA, ³School of Physics and Astronomy, University of Leicester, Leicester, UK, ⁴Department of Physics, Aberystwyth University, Aberystwyth, UK, ⁵Department of Meteorology, Space and Atmospheric Electricity Group, Reading, UK, ⁶Blackett Laboratory, Imperial College London, London, UK, ⁷Department of Astronomy, University of California, Berkeley, CA, USA, ⁸LIRA, Observatoire de Paris, Université PSL, CNRS, Sorbonne Université, Université Paris Cité, Meudon, France, ⁹Physics Department, Lancaster University, Lancaster, UK

Abstract Past observations of Saturn's sub-auroral ionosphere have provided no detailed longitudinal information, and variations in underlying stratospheric emission from methane fluorescence have never been resolved spatially. Here, we present the first near-infrared observations of Saturn using JWST's NIRSpec-IFU, revealing the 2.8–5.2 micron wavelength region in unprecedented detail. We observe the rotating auroral enhancement associated with planetary-period currents, the phase of which is re-discovered for the first time since Cassini. We discover a series of ionospheric dark beads located between 55 and 65°N, that appear to be formed by local thermospheric dynamics. In the fluorescing methane, we reveal strange dark arms extending equatorward from a dark polar cap at 60°N; four arms from a six-pointed star, each extend below 45°N with the final two arms missing. Neither set of features has any known analog at other planets.

Plain Language Summary Saturn's upper atmosphere is very poorly understood. Despite decades of ground-based observations and a decade of measurements from Cassini, the incredibly weak emission from both ions and neutrals in the top of Saturn's atmosphere have proven highly illusive. Here, we describe revolutionary observations made by the JWST telescope. The incredible sensitivity of JWST/NIRSpec allows us to measure both the ionosphere and stratosphere enhanced by orders of magnitude compared to past observations. We have discovered a series of ionospheric dark 'beads', forming across a range of longitudes, away from the region with brightest aurora. We suggest it is unlikely that they are driven by underlying atmospheric processes, or infalling material from the surrounding space environment, and speculate they are forming as a result of shears between ionospheric winds. Underlying this, the upper stratosphere appears to have an atmospheric formation unlike anything previously known. A dark polar cap appears to be extending arms down into the sub-equatorial region, with spokes reaching out as a six-pointed star. However, two of these six arms are missing, resulting in a strangely asymmetric structure. We cannot explain how this structure has formed, but it may be associated with changes seen in the underlying atmosphere.

1. Introduction

Saturn's main auroral emission produces a wide array of different small-scale structures (Grodent, 2015), but in overall morphology is dominated by two different sources of emission: a solar-wind-magnetosphere-associated aurora (Cowley et al., 2004) and a longitudinally-aligned aurora driven by the flow of the neutral atmosphere (G. J. Hunt et al., 2014; Chowdhury et al., 2022).

When averaged over multiple days, Saturn's aurora is brightest in the dawn-noon sector in both ultraviolet (UV) (Lamy et al., 2009) and within infrared emission from the ionic molecule H_3^+ (Badman et al., 2011), resulting from short-term, bright, dawn storm events caused by magnetotail reconnection. However, the median auroral emission, under more typical conditions, is brightest in the dusk-midnight sector (Bader et al., 2019).

Overlaying this local-time dominated aurora sits a second aurora, rotating with the planet, produced by a current system powered by neutrals flowing faster than, and thus dragging, ions within the ionosphere (Smith, 2011). This

Visualization: Tom S. Stallard, Imke de Pater
Writing – original draft: Tom S. Stallard, Leigh Fletcher
Writing – review & editing: Tom S. Stallard, Luke Moore, Henrik Melin, Omakshi Agiwal, M. Nahid Chowdhury, Rosie E. Johnson, Katie L. Knowles, Emma M. Thomas, Paola I. Tiranti, James O'Donoghue, Khalid Mohamed, Ingo Mueller-Wodarg, Leigh Fletcher, Imke de Pater, Thierry Fouchet, Sarah V. Badman

drives currents out into the surrounding magnetosphere, where it is observed across a wide range of locations (Carbary et al., 2018). Where local-time currents flow in the same direction as this 'planetary-period current', the aurora is significantly enhanced, but where they oppose one another, the currents cancel out, leaving greatly weakened aurora (G. J. Hunt et al., 2014).

Equatorward of the main aurora, the UV emission includes a midnight arc of emission, associated with diffuse precipitation of energetic particles (Grodent et al., 2010), localized spots of emission related to magnetospheric injections (Radioti et al., 2013), and, on rare occasions (~2%), a weak spot at the magnetic footprint of the moon Enceladus (Pryor et al., 2011).

However, in H_3^+ emission, the sub-auroral regions are typically dominated by the consequences of infalling charged and neutral ring particles, traveling along magnetic field lines and gravitationally into the equator respectively (O'Donoghue et al., 2013; Waite et al., 2018). These particles act to chemically modulate H_3^+ , increasing H_3^+ densities at moderate infall rates, then significantly decreasing H_3^+ densities at higher infall rates (Moore et al., 2015). This results in bands of H_3^+ enhancement and destruction at specific magnetic latitudes mapping to ring-particle sources within Saturn's magnetosphere (O'Donoghue et al., 2013, 2019).

However, all studies of the non-auroral ionosphere of Saturn either measure specific ray-path locations using radio occultations (e.g., Mendillo et al., 2018; Tamburo et al., 2023) or combine many hours of ground-based observation to measure the H_3^+ emission (e.g., O'Donoghue et al., 2013). As a result, no detailed maps of ionospheric sub-auroral morphology exist.

Beneath the H_3^+ ionosphere (peaking at 1,150 km (T. S. Stallard et al., 2012);) sits a layer of fluorescing methane (at ~600 km; Kim et al., 2019). Unlike Jupiter, where fluorescing methane is strongly enhanced by the aurora (Kim et al., 2009), no auroral enhancement has been observed at Saturn. Away from the aurora, only disk-wide methane fluorescence measurements have been made (Drossart et al., 1999), with spatial measurements again limited by the difficulty in detecting this weak emission.

Here, we utilize the first observations of Saturn's auroral H_3^+ made by JWST, to observe Saturn's sub-auroral ionosphere in detail.

2. Observations

The JWST NIRSpec-IFU observed Saturn's northern auroral region with its 30×30 0.1-arcsec-pixel field of view. Using the F290LP/G395H filter/grating, wavelengths between 2.86 and 5.27 micron were observed at a spectral resolution of $R \approx 4,700$, producing 3,623 individual wavelength elements. The Northern auroral region was observed continuously through a Saturnian day, between 04:00-13:58 UT on 29 November 2024. A 4-point ~1.6 arcsec dither provided an effective coverage of 5×5 arcsec per set of 4 individual observations, resulting in 26 sets and 104 individual dithers. We remove the top and bottom three rows from each dither, since these are often corrupted by bad pixels.

Figure 1 shows how, from this wide range of wavelengths, we pick specific wavelengths to build a range of images of Saturn, used in Video 1 and Figure 2:

1. Reflected sunlight (gray; Figure 1a) takes the median brightness between 3.0 and 3.2 microns.
2. Thermal emission from the planet's interior (red in Figure 1b), takes the median brightness between 5.0 and 5.2 microns.
3. For fundamental methane fluorescence, we:
 - (a) add light between wavelengths 3.3129–3.3155 micron (blue; Figure 1c);
 - (b) and subtract nearby background emission between 3.3082 and 3.3109 microns (purple; Figure 1d).
4. For H_3^+ emission, we:
 - (a) sum H_3^+ dominated wavelengths (green; Figure 1e): 3.5330, 3.5336, 3.5383, 3.5389, 3.9040, 3.9533, and 4.3503 microns;
 - (b) take nearby background light (purple; Figure 1f) from wavelengths: 3.5290, 3.5297, 3.9061, 3.9021, 3.9519, 4.3483, and 4.3516 microns;
 - (c) and factor the background light by the values: 1, 2, 0.5, 0.5, 0.0768, 0.595, and 0.4 respectively, before subtracting their sum from the H_3^+ image.

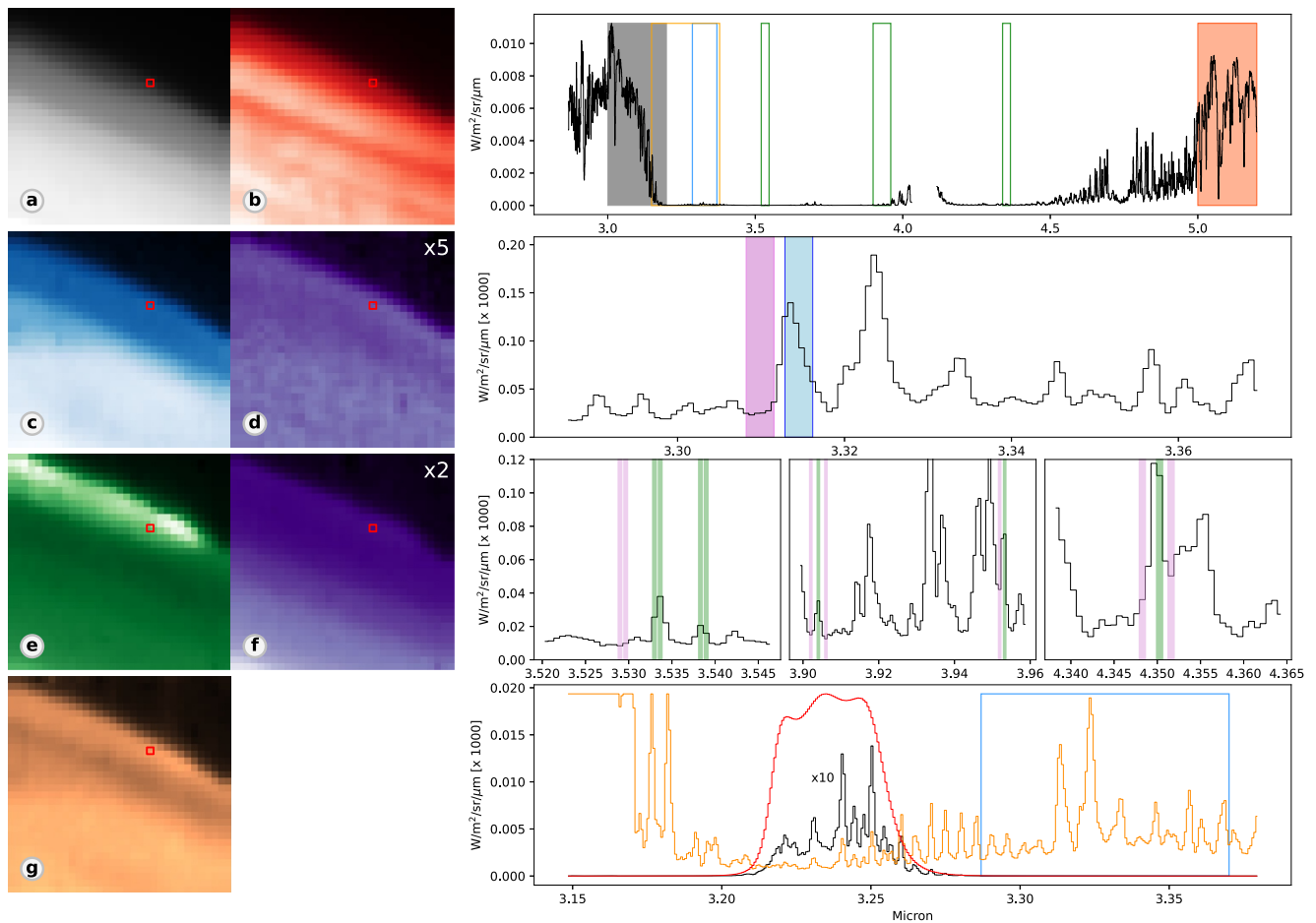


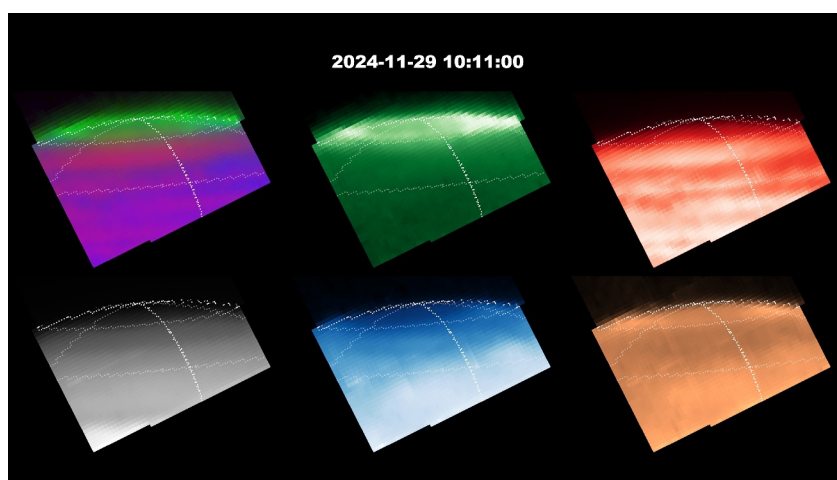
Figure 1. Saturn images from dither 18/104. On the left, individual dithers are colored based upon the wavelengths they represent; on the right, matching spectral windows are plotted. (a) The median emission from reflected sunlight observed between 3.0 and 3.2 micron. (b) Thermal emission released from Saturn, observed between 5.0 and 5.2 micron. Right of this is the full auroral spectrum measured at pixel 20x, 20y (red box in each image). Wavelengths used in (a) and (b) are highlighted in gray and red; wavelengths of the underlying panels are outlined in appropriate colors. (c) Emission from methane fundamental fluorescence; (d) nearby background emission, scaled up by a factor of 2; to the right, wavelengths used are highlighted in blue and purple respectively. (e) The summed emission from H_3^+ bright wavelengths; (f) nearby background emission scaled up by a factor of 2; on the right, H_3^+ and background wavelength regions used are highlighted in green and purple, across three separate windows. (g) A modeled NIRCам-F323N filter image for comparison with past observations; on the right, the spectrum (orange) is factored against the F323N filter transparency (red) to produce an observable spectrum.

5. JWST's NIRCам-F323N filter (orange; Figure 1g) is emulated by factoring the observed spectra against the F323N filter transmission. This can be directly compared with the GTO-1247 Saturn image, released in June 2023.

Video 1 shows a video of the full sequence of four-dither images, highlighting emission from thermal emission (red), H_3^+ emission (green); methane fundamental fluorescence (blue); the emulated image observed by NIRCам-F323N (orange).

This highlights two important details. Firstly, the H_3^+ auroral emission is dominated by a localized enhanced region rotating with the planet without any clear local time fixed auroral enhancements. This strongly suggests that dynamic magnetospheric forcing was relatively quiescent during these observations, with auroral variability dominated, instead, by the atmospherically-driven planetary-period aurora. Secondly, images of the methane fundamental fluorescence provide a spatially resolved distribution, consisting of brighter equatorial emission and a darker region across the polar cap, with complex morphology sweeping past our field of view.

We then map the observations into Saturnian latitude and longitude, by calculating the latitudinal and longitudinal coordinates of every pixel corner within each of the 104 individual dithers. These pixel brightnesses are transferred into a 0.5° resolution latitude/longitude map of Saturn: we calculate the proportion of each latitude-



Video 1. The observed emission across a Saturnian day observed by JWST. Each panel shows a sequence of 26 dither-combined images at the North pole of Saturn, with a frame rate of ~ 100 min per second, with 10° latitude and 45° longitude steps demarked. Top left: a three-color image combining thermal (red), H_3^+ (green), and CH_4 fundamental emission (blue); top center: H_3^+ emission, square-rooted to highlight weaker intensities (green); top right: thermal emission between 5.0 and 5.2 micron (red). Bottom left: reflected sunlight observed between 3 and 3.2 micron (grayscale); Bottom center: methane fundamental fluorescence (blue); bottom right: emulated NIRC_{Cam}-F323N observation (orange). All images have been normalized. The start date and time for each four-dither image is show at the top.

longitude bin filled by each pixel, adding that proportion of the pixel intensity to the map and recording that proportion to a second “count” map. As a result, we produce two maps, one containing the combined proportional intensities and the other the proportional counts from these pixels. Dividing one by the other, we produce a final mean intensity map.

Figure 2 shows polar plots of Saturn's northern auroral region. In Figure 2a, the mapped Northern auroral morphology is clearly revealed. The H_3^+ emission peaks at a System III longitude (Archinal et al., 2018) of $\sim 130^\circ\text{W}$ and close to 75°N , the main emission at this latitude extending most obviously from 60 to 240°W . A second region of enhanced H_3^+ emission is observed between 270 and 165°W at close to 75°N . Figure 2b highlights the auroral structure even more clearly by removing the longitudinal H_3^+ median brightness from each individual latitude slice. Here, two regions of H_3^+ morphology are clearly revealed near 75°N : the first, the positive values (red) identified above, the second a morphologically matching negative (blue) feature, both consisting of a narrow peak surrounded by a fading long bar either side. Notably, the emission matches the median emission (white) at quadrature with this minimum and maximum.

The mirrored quadrature nature of the morphology, along with its peak close to 75°N , both strongly indicate the morphology in Figure 2a is produced by an approximately axisymmetric middle-magnetospheric auroral current modulated by a rotating planetary-period auroral current, highlighted in Figure 2b, positioned with respect to the northern planetary-period oscillation phase Ψ_N , as defined in G. Hunt et al., 2015. This would enhance upward auroral currents at a planetary-period phase of $90^\circ\Psi_N$ and mitigate upward auroral currents with downward planetary-period currents, reducing the overall auroral brightness, at a planetary-period phase of $270^\circ\Psi_N$, seen as the planet rotates in Video 1. Notably, for a single rotation, the planetary-period rotation rate is effectively very close to the IAU rotation period (10 hr 39 m 22.4 s).

Other auroral processes, not seen here (such as dawn enhancements, or plasma injections), typically rotate more slowly than the planet, and only occur at some local times, suggesting our JWST observations were taken at a period of very low magnetospheric variability, with brightness changes dominated by atmospherically-driven currents. Assuming this, we estimate the northern planetary-period Phase $0^\circ\Psi_N$ was at IAU longitude of 55°W during these observations (a value lost since Cassini), denoted using a pink dotted lines in Figures 2b and 2g. However, this phase should be considered an estimate: Bader et al. (2018) showed the UV peak lags the model current peak by $\sim 30^\circ\Psi_N$, and Badman et al. (2012) found a different (leading) result for the H_3^+ intensity peak.

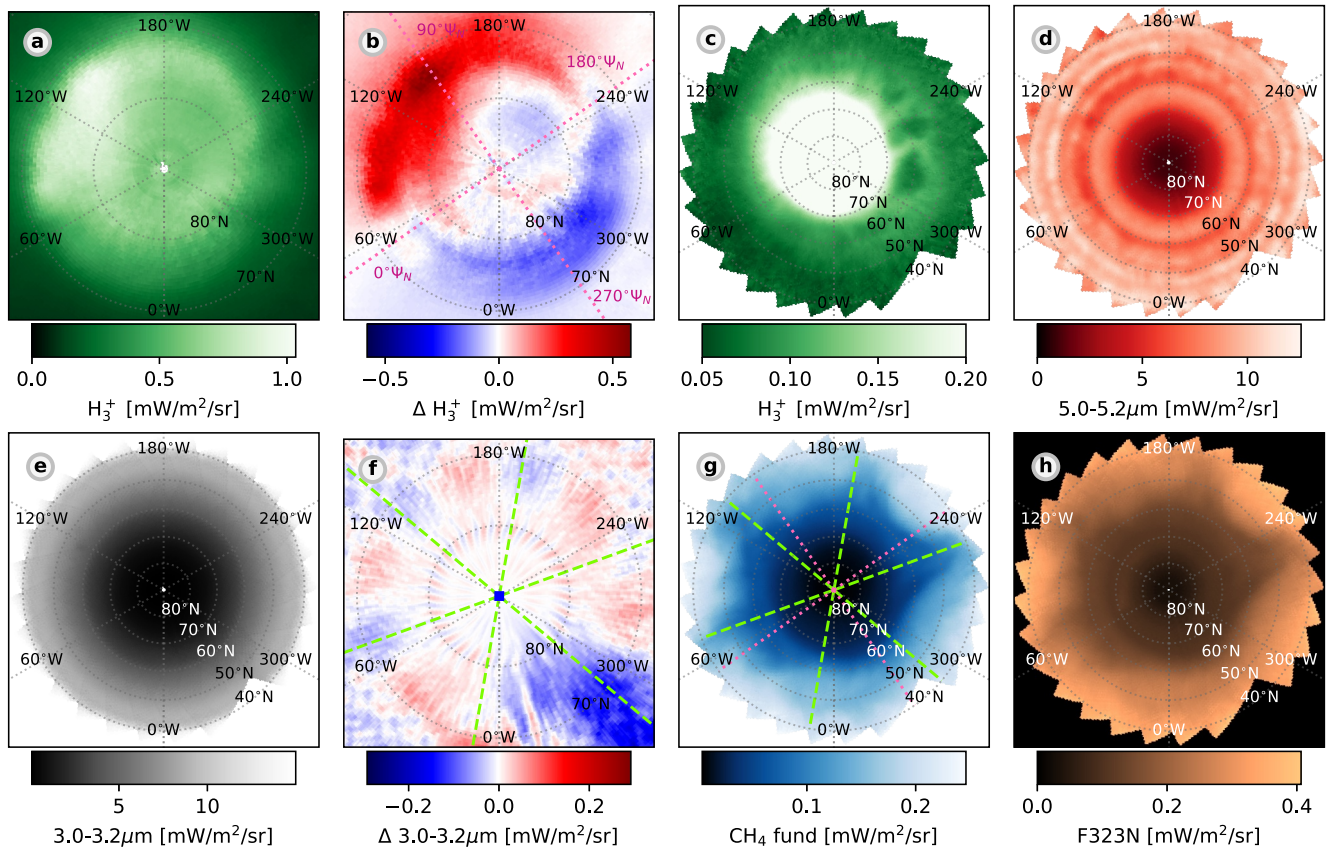


Figure 2. Saturn's northern polar region at various wavelengths. In all plots, latitude is demarked every 10° and longitude every 60°, and all brightnesses are in mW/m²/sr. (a) H₃⁺ emission (green) inside 68°N. (b) H₃⁺ emission with the median longitudinally averaged emission subtracted, showing ΔH_3^+ brightness for each latitudinal band. We have assigned a planetary-period phase, highlighted with pink dotted line. (c) The full H₃⁺ emission map, here, ranging between 0.05 and 0.2 mW/m²/sr (~5–20% the peak emission), revealing the sub-auroral ionospheric structure. (d) Median thermal emission between 5.0 and 5.2 (red). (e) Median reflected sunlight between 3.0 and 3.2 micron (gray). (f) Reflected sunlight inside 68°N with the median longitudinally-averaged emission subtracted, showing brightness difference, smoothed by a 2° boxcar for clarity; at a latitude of ~70°N, the signature of Saturn's northern hexagon can be seen as alternating positive and negative values, highlighted at negative values using green dashed lines. (g) Fundamental methane fluorescence (blue), with both the planetary-period phase (pink dotted lines) and hexagon phase (green dashed lines) overplotted. (h) Emulated emission that NIRCam-F323N would have observed.

Figure 2c reveals localized morphology within Saturn's sub-auroral region for the first time. The expectation was bands of “Ring-rain” brightening and darkening within latitudes, magnetically mapping to heavy ion sources within the surrounding magnetosphere. However, no clear banding exists here. O'Donoghue et al. (2017) showed that the intensity of H₃⁺ variability was strongly seasonally modulated, with no clear E-ring signature 16 months after equinox. The lack of a clear H₃⁺ enhancement here confirms that measurement, likely a direct response to the seasonal weakening of ring ionosphere's plasma density close to equinox, where the edge-on rings receive significantly less ionizing sunlight (Persoon et al., 2015). These JWST observations were taken only 6 months before equinox, where infalling ring plasma density in the northern ionosphere should be close to zero (Tseng et al., 2011).

However, unexpectedly, the sub-auroral region contains very significant localized variations. A series of dark beads in a variety of sizes and shapes, only occurring on one side of the ionosphere, between ~180–0°W, with the largest and darkest beads between 240 and 300°W. No known ionospheric planetary analog exists for these features, and we speculate these unique structures might:

1. Represent the imprint of underlying atmospheric dynamics or heating;
2. be intrinsic to the ionosphere or thermosphere themselves;
3. or be produced through the influence of magnetospheric sources.

Away from these dark beads, the sub-auroral H_3^+ emission is brightest at longitudes where the main aurora is also brightest.

Figure 2d and e show the deep underlying atmosphere (thermal emission from below the clouds and reflected sunlight from the cloud layers respectively), neither of which show significant matching atmospheric features. Saturn's northern hexagon, last clearly observed in the thermal emission in 2017 (Blake et al., 2023), cannot be seen here. However, by subtracting the median sunlight brightness, shown in Figure 2f, we are able to identify six bright and dark patches that reveal the signature of the hexagon, the phase of which is delineated by green dashed lines.

The highest atmospheric layer identified beneath Saturn's H_3^+ ionosphere are fluorescing methane emissions previously shown to peak in emission close to 600 km (Kim et al., 2019). The spatial morphology of this region has not previously been observed, due to sensitivity limitations. In Figure 2g we reveal a highly asymmetric morphology, with a dark polar cap at $\sim 60^\circ N$, but extending down to at least $40^\circ N$ along only four arms of a six-pointed star shape, with the other two arms missing. This stratospheric structure is again unlike anything previously observed at other planets. While we do not understand how or why these dark arms are generated, it is perhaps noteworthy that they occur in a region where the underlying atmosphere is also disturbed (Figure 2f), suggesting this stratospheric layer might be influenced from below.

The field of view in these observations is too small to constrain the equatorward extent of these polar darkening extensions. However, the same structures can be observed in Figure 2h, emulating JWST's NIRC2-F323N filter (Rieke et al., 2023), as imaged by GTO-1247 and released in a press release in June 2023. That image showed clear asymmetries in the measured brightness down to at least $45^\circ N$, but did not appear to extend down to the equator in that image. That image also appeared to show faint auroral structure near the poles. Detailed investigation of the auroral emission in this region (see Text S1 in Supporting information S1) suggests the auroral enhancement is only $\sim 1/10$ H_3^+ emission, but still has the same morphology as H_3^+ emission, so future observations of Saturn with the F323 N filter could provide spatial information for both auroral and stratospheric dynamics.

Saturn's thermospheric dynamics, revealed in both ion winds (Chowdhury et al., 2022) and theories explaining planetary-period oscillations in the magnetosphere (Smith, 2006; G. J. Hunt et al., 2014; Jia et al., 2012), require a neutral twin-cell vortex positioned over the pole, with a sub-auroral super-rotating wind strongest at $270^\circ \Psi_N$, a sub-auroral sub-rotating wind strongest at $90^\circ \Psi_N$, and a polar return flow from $180^\circ \Psi_N$ to $0^\circ \Psi_N$. While the depth of this flow is unknown, assuming our phase is correctly assigned, the shape of the features observed in Figure 2g do not match well with such shearing; the lack of equatorward flows at $270^\circ \Psi_N$ might instead suggest a poleward Coriolis force driven by super-rotating flows. This strongly suggests this layer of the stratosphere is independent from the thermospheric twin-cell vortex.

As such, there is little evidence of the dark beads in H_3^+ being driven by the underlying atmosphere, though there remains a ~ 400 km region of Saturn's atmosphere (650–1,050 km; Kim et al., 2019, or 2–3 pressure-decades; Iñurrigarro et al., 2024), above the fluorescing methane and below the H_3^+ , that contains no emissive species yet examined in detail.

At Jupiter, significant localized dark spots are observed (T. S. Stallard et al., 2018). Although previously speculated to be driven by dynamic thermospheric interactions (T. S. Stallard et al., 2017), these have recently been shown to occur in regions of higher-order magnetic features (Knowles et al., 2025). Saturn's much more (albeit offset) dipolar magnetic field (Dougherty et al., 2018) suggest comparable features would struggle to form here.

The beads are strongest at planetary-period phases between 180 and $270^\circ \Psi_N$. Since the planetary-period twin-cell vortex super-rotates in this region, against the general trend of sub-rotational flows between $65^\circ N$ and the pole, perhaps the imposition of these two counter flows could form Kelvin-Helmholtz instabilities along the boundary. Indeed, although Chowdhury et al. (2022) considered differences between the flows observed at $90^\circ \Psi_N$ and $270^\circ \Psi_N$ to be the result of dusk auroral activity on some nights, the observed ion flows revealed a clean and strong return sub-rotation at $90^\circ \Psi_N$ but fragmented weakened return super-rotation at $270^\circ \Psi_N$. This, in turn, aligns with the weaker auroral darkening (caused by weaker downward currents) at $270^\circ \Psi_N$ observed here, shown in blue in Figure 2b.

Finally, the dark beads may be produced by morphologically complex infalling material from the E-ring. However, the E-ring is longitudinally smooth and tightly confined in radial distance from Saturn (Hedman

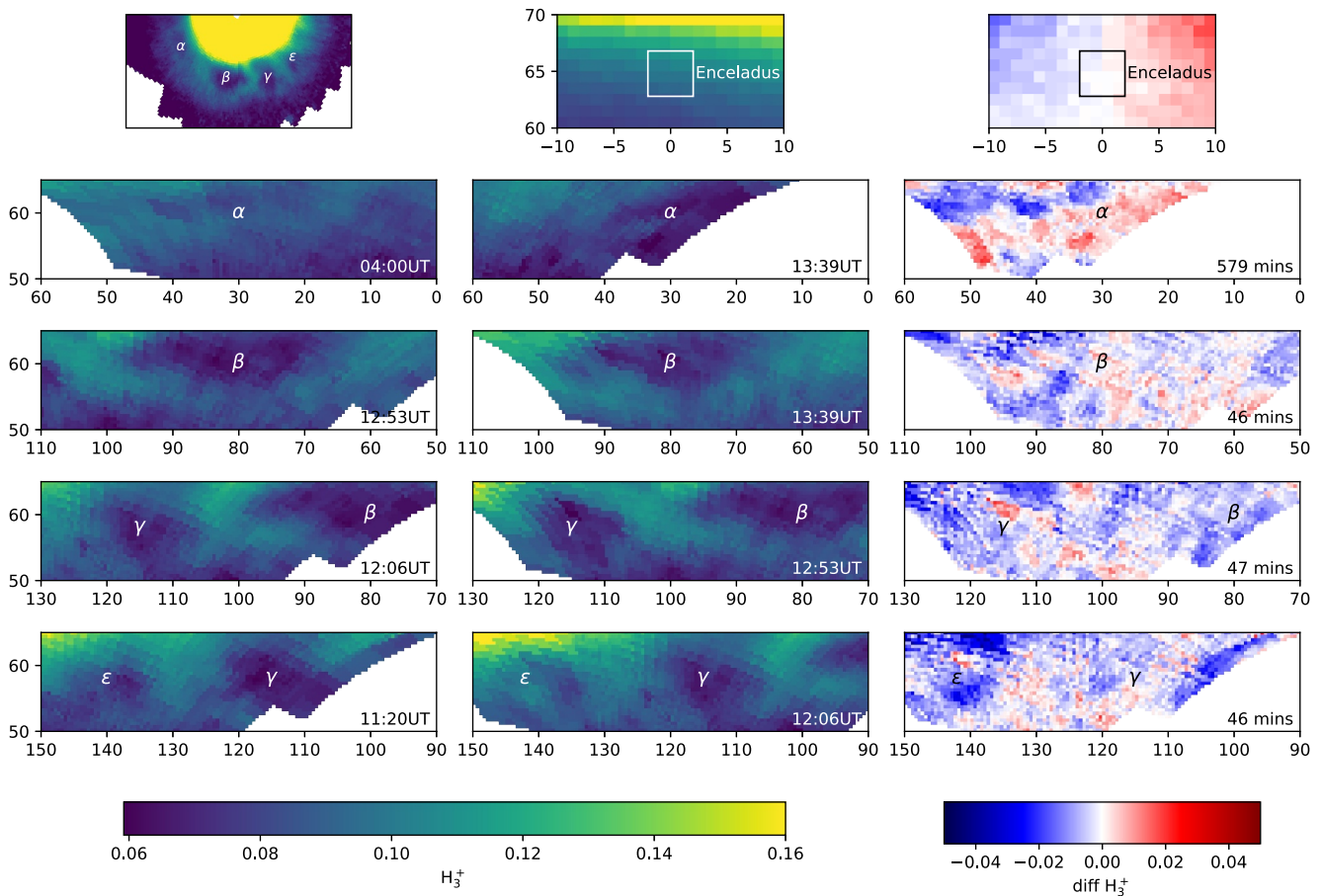


Figure 3. Saturn's sub-auroral ionospheric features. Top left shows a polar map of the sub-auroral region (comparable with Figure 2c, here rotated 90°E), with the four beads highlighted, demarked with a letter for identification: α , β , γ and ϵ . All other panels are plotted in plate carrée projection, west longitude in the x-axis and latitude in the y-axis. Top middle shows the mean average emission across every individual image positioned on the latitude and longitudinal location of Enceladus. Top right shows the same emission with the median latitudinal brightness removed. Below this, the next four rows each show two sets of individual mapped images. The second row shows the first and last image, with a small overlap in longitudes, while the third to fifth rows each have two images (separated by a missing middle image, not shown). These map out the same sub-auroral features, with the right column showing the difference in brightness between these two images.

et al., 2012), so the expectation would be the strongest ionospheric reactions should occur along all longitudes at the magnetically mapped latitude of Enceladus (64.8°N).

In Figure 3, we examine both the positioning and variability of the sub-auroral ionosphere. In the center of the top row, we map the exact latitude and longitude of Enceladus in each of the 104 images, taking the mean emission across a range of $\pm 10^\circ$ longitude and $\pm 5^\circ$ latitude. The resultant ionospheric emission is brighter at higher longitudes: because Enceladus was only visible between $\sim 350^\circ\text{W}$ and $\sim 140^\circ\text{W}$, where there is a westward bias in auroral brightness. Once the median brightness with latitude is removed (shown in the top right of Figure 3), no ionospheric response is measured from Enceladus, either from the E-ring across longitudes at 64.8°N, or from an enhanced spot at the magnetic footprint of Enceladus. Using the standard deviation of values within 3° of the spot, we estimate an upper limit Enceladus spot brightness of $<0.15\%$ the peak auroral emission.

The bottom four rows of Figure 3 show a region equatorward of the Enceladus mapping, away from sub-auroral brightening, mapped in individual longitudinal regions from five images, each made from four individual dithers. The second row shows overlapping images from the start and end of the observation, separated by nearly 10 hr. Here, there is a single narrow darkening (α). At 04:00 UT, this was positioned between 20 and 40°W and $\sim 61^\circ\text{N}$. Ten hours later, at 13:39 UT, the α feature appears to have moved slightly equatorward, to 20–40°W and $\sim 59^\circ\text{N}$. In rows 3–5 of Figure 3, we observe changes in structure over a shorter period of ~ 46 min. At this cadence, the overall structure of features β , γ and ϵ are relatively constant, with variation typically $<10\%$ the brightness of this region and $<1\%$ the peak auroral brightness.

The β and γ beads are strongest, eastward of the two missing methane star arms. However, if driven from this underlying atmosphere, the features must be driven by deeply penetrating winds. If they were local to thermosphere, α would be swept super-rotationally eastwards by the planetary-period neutral flows, with ion winds observed by Chowdhury et al. (2022) predicting a $\sim 45^\circ\text{E}$ motion in this time-frame.

3. Conclusions

The weak emission from Saturn's sub-auroral ionosphere has always been challenging to observe, preventing spatially resolved observations from either Cassini or ground-based observatories. In this context, JWST has revolutionized our understanding of the sub-auroral ionosphere.

It has revealed complex dark beads in the $50\text{--}65^\circ\text{N}$ region, slightly equatorward of Enceladus's magnetically-mapped location. These beads are dynamically stable over hour-long timescales, but appear to move by a few degrees over a Saturnian day, suggesting a longer-term instability. They do not appear to be well correlated with any underlying dynamics or magnetospheric sources, strongly suggesting they result from dynamics within the thermosphere (or closely confined underlying atmospheric layers). They occur in a region where the planetary-period currents produces flows counter to the prevailing polar sub-rotation, suggesting these features may be generated by the complex interplay between the surrounding magnetosphere and dynamic atmosphere, and may provide a trace of the energy interchange that powers the pulsing of Saturn's aurora.

Ultimately, this new form of ionospheric feature may provide a planetary context to the complex swirling of Earth's thermosphere (Walterscheid & Crowley, 2015), as well as the potentially complex interactions within Jupiter and the Ice Giants ionospheres, only now coming to light with the focus of JWST upon them (Melin et al., 2025).

Inclusion in Global Research Statement

A clear understanding was reached among collaborators with regard to their roles, responsibilities and conduct throughout the research cycle, from study design through to study implementation, review and dissemination. We have included all contributors to the JWST proposal, which included academics from all stages of career from PhD student to professor.

Data Availability Statement

Data used in this publication is currently under embargo and so is not yet available from MAST. After 29 November 2025, the raw data will be available to download (https://mast.stsci.edu/search/ui/#/jwst/results?program_id=5308). Complementary to these raw files, we have uploaded each of the 104 individual dithers having undergone partial pipeline processing (the extend of processing used in this paper). We have also uploaded the data cube used in this study, combining wavelength with a 0.5° latitude and longitude binning. There are available from the Harvard Dataverse (T. Stallard, 2025).

Acknowledgments

T.S., E.M.T. and L.N.F. were supported by the STFC Consolidated Grant (ST/W00089X/1). H.M. was supported by the STFC James Webb Fellowship (ST/W001527/2). L.M. was supported by Grant 80NSSC20K1045 issued through the NASA Solar System Workings program. L.N.F. was supported by a European Research Council Consolidator Grant under the European Union's Horizon 2020 research and innovation program, Grant agreement 723890. J. O'D. was supported by the STFC Ernest Rutherford Fellowship (ST/X003426/1). P.I.T. was supported by a STFC PhD studentship Grant (ST/X508548/2). K.L.K. was supported by a Northumbria University Research Studentship. O.A. acknowledges support by NASA Grant 80NSSC21K0157 issued through the Solar System Workings Program.

References

- Archinal, B. A., Acton, C. H., A'Hearn, M. F., Conrad, A., Consolmagno, G. J., Duxbury, T., et al. (2018). Report of the IAU working group on cartographic coordinates and rotational elements: 2015. *Celestial Mechanics and Dynamical Astronomy*, 130(3), 22. <https://doi.org/10.1007/s10569-017-9805-5>
- Bader, A., Badman, S., Kinrade, J., Cowley, S., Provan, G., & Pryor, W. (2018). Statistical planetary period oscillation signatures in Saturn's UV auroral intensity. *Journal of Geophysical Research: Space Physics*, 123(10), 8459–8472. <https://doi.org/10.1029/2018ja025855>
- Bader, A., Badman, S., Cowley, S., Yao, Z., Ray, L. C., Kinrade, J., et al. (2019). The dynamics of Saturn's main aurorae. *Geophysical Research Letters*, 46(17–18), 10283–10294. <https://doi.org/10.1029/2019gl084620>
- Badman, S. V., Andrews, D. J., Cowley, S., Lamy, L., Provan, G., Tao, C., et al. (2012). Rotational modulation and local time dependence of Saturn's infrared H_3^+ auroral intensity. *Journal of Geophysical Research*, 117(A9). <https://doi.org/10.1029/2012ja017990>
- Badman, S. V., Tao, C., Grocott, A., Kasahara, S., Melin, H., Brown, R. H., et al. (2011). Cassini VIMS observations of latitudinal and hemispheric variations in Saturn's infrared auroral intensity. *Icarus*, 216(2), 367–375. <https://doi.org/10.1016/j.icarus.2011.09.031>
- Blake, J. S. D., Fletcher, L. N., Orton, G. S., Antuñano, A., Roman, M. T., Kasaba, Y., et al. (2023). Saturn's seasonal variability from four decades of ground-based mid-infrared observations. *Icarus*, 392, 115347. <https://doi.org/10.1016/j.icarus.2022.115347>
- Carbary, J. F., Hedman, M. M., Hill, T. W., Jia, X., Kurth, W., Lamy, L., & Provan, G. (2018). The mysterious periodicities of Saturn. *Saturn in the 21st Century*, 20, 97–125. <https://doi.org/10.1017/9781316227220.005>
- Chowdhury, M., Stallard, T., Baines, K., Provan, G., Melin, H., Hunt, G., et al. (2022). Saturn's weather-driven aurorae modulate oscillations in the magnetic field and radio emissions. *Geophysical Research Letters*, 49(3), e2021GL096492. <https://doi.org/10.1029/2021gl096492>

- Cowley, S., Bunce, E., & Prangé, R. (2004). Saturn's polar ionospheric flows and their relation to the main auroral oval. *Annales Geophysicae*, 22(4), 1379–1394. <https://doi.org/10.5194/angeo-22-1379-2004>
- Dougherty, M. K., Cao, H., Khurana, K. K., Hunt, G. J., Provan, G., Kellock, S., et al. (2018). Saturn's magnetic field revealed by the Cassini grand finale. *Science*, 362(6410), aat5434. <https://doi.org/10.1126/science.aat5434>
- Drossart, P., Fouchet, T., Crovisier, J., Lellouch, E., Encrenaz, T., Feuchtgruber, H., & Champion, J. P. (1999). Fluorescence in the 3 μ m bands of methane on Jupiter and Saturn from ISO/SWS observations. In P. Cox & M. Kessler (Eds.), *The universe as seen by iso* (Vol. 427), 169.
- Grodent, D. (2015). A brief review of ultraviolet auroral emissions on giant planets. *Space Science Reviews*, 187(1–4), 23–50. https://doi.org/10.1007/978-1-4939-3395-2_3
- Grodent, D., Radioti, A., Bonfond, B., & Gérard, J.-C. (2010). On the origin of Saturn's outer auroral emission. *Journal of Geophysical Research (Space Physics)*, 115(A8), A08219. <https://doi.org/10.1029/2009JA014901>
- Hedman, M. M., Burns, J. A., Hamilton, D. P., & Showalter, M. R. (2012). The three-dimensional structure of Saturn's E ring. *Icarus*, 217(1), 322–338. <https://doi.org/10.1016/j.icarus.2011.11.006>
- Hunt, G., Cowley, S., Provan, G., Bunce, E., Alexeev, I., Belenkaya, E., et al. (2015). Field-aligned currents in Saturn's northern nightside magnetosphere: Evidence for interhemispheric current flow associated with planetary period oscillations. *Journal of Geophysical Research: Space Physics*, 120(9), 7552–7584. <https://doi.org/10.1002/2015ja021454>
- Hunt, G. J., Cowley, S. W., Provan, G., Bunce, E. J., Alexeev, I. I., Belenkaya, E. S., et al. (2014). Field-aligned currents in Saturn's southern nightside magnetosphere: Subcorotation and planetary period oscillation components. *Journal of Geophysical Research: Space Physics*, 119(12), 9847–9899. <https://doi.org/10.1002/2014ja020506>
- Iñurrigarro, P., Medvedev, A. S., Müller-Wodarg, I. C. F., & Moore, L. (2024). Aurorally driven supersonic gravity waves in Saturn's atmosphere. *Geophysical Research Letters*, 51(19), e2024GL110883. <https://doi.org/10.1029/2024GL110883>
- Jia, X., Kivelson, M. G., & Gombosi, T. I. (2012). Driving Saturn's magnetospheric periodicities from the upper atmosphere/ionosphere. *Journal of Geophysical Research*, 117(A4). <https://doi.org/10.1029/2011ja017367>
- Kim, S. J., Geballe, T. R., Seo, H. J., & Kim, J. H. (2009). Jupiter's hydrocarbon polar brightening: Discovery of 3-micron line emission from south polar CH₄, C₂H₂, and C₂H₆. *Icarus*, 202(1), 354–357. <https://doi.org/10.1016/j.icarus.2009.03.020>
- Kim, S. J., Sim, C. K., Stallard, T. S., & Courtin, R. (2019). Spectral characteristics and formation of high-altitude haze in the south-polar regions of Saturn. *Icarus*, 321, 436–444. <https://doi.org/10.1016/j.icarus.2018.12.004>
- Knowles, K. L., Stallard, T. S., O'Donoghue, J., Moore, L., Agiwal, O., Melin, H., et al. (2025). Magnetic silhouettes in Jupiter's non-auroral ionosphere. *Journal of Geophysical Research (Space Physics)*, 130(5), e2025JA033868. <https://doi.org/10.1029/2025JA033868>
- Lamy, L., Cecconi, B., Prangé, R., Zarka, P., Nichols, J., & Clarke, J. (2009). An auroral oval at the footprint of Saturn's kilometric radio sources, collocated with the UV aurorae. *Journal of Geophysical Research*, 114(A10), A10212. <https://doi.org/10.1029/2009ja014401>
- Melin, H., Moore, L., Fletcher, L. N., Hammel, H. B., O'Donoghue, J., Stallard, T. S., et al. (2025). Discovery of H₃⁺ and infrared aurorae at Neptune with JWST. *Nature Astronomy*, 9(5), 666–671. <https://doi.org/10.1038/s41550-025-02507-9>
- Mendillo, M., Trovato, J., Moore, L., & Müller-Wodarg, I. (2018). Comparative ionospheres: Terrestrial and giant planets. *Icarus*, 303, 34–46. <https://doi.org/10.1016/j.icarus.2017.12.033>
- Moore, L., O'Donoghue, J., Müller-Wodarg, I., Galand, M., & Mendillo, M. (2015). Saturn ring rain: Model estimates of water influx into Saturn's atmosphere. *Icarus*, 245, 355–366. <https://doi.org/10.1016/j.icarus.2014.08.041>
- O'Donoghue, J., Moore, L., Connerney, J., Melin, H., Stallard, T. S., Miller, S., & Baines, K. H. (2019). Observations of the chemical and thermal response of "ring rain" on Saturn's ionosphere. *Icarus*, 322, 251–260. <https://doi.org/10.1016/j.icarus.2018.10.027>
- O'Donoghue, J., Moore, L., Connerney, J. E. P., Melin, H., Stallard, T. S., Miller, S., & Baines, K. H. (2017). Redetection of the ionospheric H₃⁺ signature of Saturn's "Ring Rain". *Geophysical Research Letters*, 44(23), 11762–11769. <https://doi.org/10.1002/2017GL075932>
- O'Donoghue, J., Stallard, T. S., Melin, H., Jones, G. H., Cowley, S. W. H., Miller, S., et al. (2013). The domination of Saturn's low-latitude ionosphere by ring rain. *Nature*, 496(7444), 193–195. <https://doi.org/10.1038/nature12049>
- Persoon, A. M., Gurnett, D. A., Kurth, W. S., Groene, J. B., & Faden, J. B. (2015). Evidence for a seasonally dependent ring plasma in the region between Saturn's A ring and enceladus' orbit. *Journal of Geophysical Research (Space Physics)*, 120(8), 6276–6285. <https://doi.org/10.1002/2015JA021180>
- Pryor, W. R., Rymer, A. M., Mitchell, D. G., Hill, T. W., Young, D. T., Saur, J., et al. (2011). The auroral footprint of Enceladus on Saturn. *Nature*, 472(7343), 331–333. <https://doi.org/10.1038/nature09928>
- Radioti, A., Roussos, E., Grodent, D., Gérard, J. C., Krupp, N., Mitchell, D. G., et al. (2013). Signatures of magnetospheric injections in Saturn's Aurora. *Journal of Geophysical Research (Space Physics)*, 118(5), 1922–1933. <https://doi.org/10.1002/jgra.50161>
- Rieke, M. J., Kelly, D. M., Misselt, K., Stansberry, J., Boyer, M., Beatty, T., et al. (2023). Performance of NIRC2 on JWST in flight. *Publications of the Astronomical Society of the Pacific*, 135(1044), 028001. <https://doi.org/10.1088/1538-3873/acac53>
- Smith, C. (2006). Periodic modulation of gas giant magnetospheres by the neutral upper atmosphere. *Annales Geophysicae*, 24(10), 2709–2717. <https://doi.org/10.5194/angeo-24-2709-2006>
- Smith, C. (2011). A Saturnian cam current system driven by asymmetric thermospheric heating. *Monthly Notices of the Royal Astronomical Society*, 410(4), 2315–2328. <https://doi.org/10.1111/j.1365-2966.2010.17602.x>
- Stallard, T. (2025). Jwst observations of saturn's auroral region [dataset]. *Harvard Dataverse*. <https://doi.org/10.7910/DVN/F7ZMMW>
- Stallard, T. S., Burrell, A. G., Melin, H., Fletcher, L. N., Miller, S., Moore, L., et al. (2018). Identification of Jupiter's magnetic equator through H₃⁺ ionospheric emission. *Nature Astronomy*, 2(10), 773–777. <https://doi.org/10.1038/s41550-018-0523-z>
- Stallard, T. S., Melin, H., Miller, S., Badman, S. V., Brown, R. H., & Baines, K. H. (2012). Peak emission altitude of Saturn's H₃⁺ Aurora. *Geophysical Research Letters*, 39(15). <https://doi.org/10.1029/2012gl052806>
- Stallard, T. S., Melin, H., Miller, S., Moore, L., O'Donoghue, J., Connerney, J. E., et al. (2017). The great cold spot in Jupiter's upper atmosphere. *Geophysical Research Letters*, 44(7), 3000–3008. <https://doi.org/10.1002/2016gl071956>
- Tamburo, P., Withers, P., Dalba, P. A., Moore, L., & Koskinen, T. (2023). Cassini radio occultation observations of Saturn's ionosphere: Electron density profiles from 2005 to 2013. *Journal of Geophysical Research (Space Physics)*, 128(4), e2023JA031310. <https://doi.org/10.1029/2023JA031310>
- Tseng, W.-L., Johnson, R. E., Thomsen, M. F., Cassidy, T. A., & Elrod, M. K. (2011). Neutral H₂ and H₂⁺ ions in the saturnine magnetosphere. *Journal of Geophysical Research (Space Physics)*, 116(A3), A03209. <https://doi.org/10.1029/2010JA016145>
- Waite, J. H., Perryman, R. S., Perry, M. E., Miller, K. E., Bell, J., Cravens, T. E., et al. (2018). Chemical interactions between Saturn's atmosphere and its rings. *Science*, 362(6410), aat2382. <https://doi.org/10.1126/science.aat2382>
- Walterscheid, R. L., & Crowley, G. (2015). Thermal cell structures in the high-latitude thermosphere induced by ion drag. *Journal of Geophysical Research (Space Physics)*, 120(8), 6837–6850. <https://doi.org/10.1002/2015JA021122>